The Untold Story of Pyrocumulonimbus

Mike Fromm[1], Dan Lindsey[2], René Servranckx[3], Glenn Yue[4], Thomas Trickl[5], Robert Sica[6], Paul Doucet[6], Sophie Godin-Beekman[7]

1. Naval Research Laboratory, Washington, DC, USA.

mike.fromm@nrl.navy.mil

202 404 1389

2. NOAA, Fort Collins, CO, USA

3. Canadian Meteorological Centre, Dorval, Qubec, Canada

4. NASA Langley Research Center, Hampton, VA, USA

5. Institut für Meteorologie und Klimaforschung, Garmisch-Partenkirchen Germany

6. University of Western Ontario, London, Ontario, Canada

7. CNRS, Service d'Aeronomie, Paris, France

Capsule

Pyrocumulonimbus storms inject smoke into the stratosphere. “PyroCb” smoke has been mistaken for volcanic clouds. In one year there were at least 17 pyroCb in the USA and Canada.

Abstract

Wildfire is becoming the focus of increasing attention with heightened concerns related to climate change, global warming, and safety in the urban-wildland interface. One aspect of wildfire behavior has been totally overlooked until recently—the role of pyrocumulonimbus (pyroCb for short) in both firestorm dynamics and atmospheric impact. PyroCb are fire-started or –augmented thunderstorms that in their most extreme manifestation inject huge abundances of smoke and other biomass burning emissions into the lower stratosphere. The observed hemispheric spread of smoke and other biomass burning emissions could have important climate consequences. Such an extreme injection by thunderstorms was previously judged to be impossible because the extratopical tropopause is considered to be an effective lid on convection.

Two recurring themes have developed as pyroCb research unfolds. First, some "mystery layer" events—puzzling stratospheric aerosol layer observations— and layers reported as volcanic aerosol can now be explained in terms of pyroconvection as the "smoking gun." Secondly, pyroCb events

occur with surprising frequency, and they are likely a relevant aspect of several historic wildfires. Here we will show that pyroCbs offer an alternative explanation for previously assumed volcanic aerosols in 1989-1991. In addition, we survey the Canada/USA fire season of 2002 and identify 17 pyroCbs, some of which are associated with newsworthy fires such as Hayman, Rodeo/Chediski, and Biscuit fires. Several of these pyroCbs injected smoke into the lowermost stratosphere.

Introduction

Wildfire--and its relation to weather, climate, and society--is a topic of increasing interest and attention. For instance, the Hayman fire in Colorado in June 2002 exploded from human-caused ignition in a remote forest into a fire storm that burned 24000 ha and advanced 31 km from ignition point in its first 24 hours (Graham, 2003). Australia's capital Canberra was overwhelmed by a lightning-started bushfire in January 2003 that brought death and wholesale destruction of property (Webb et al., 2004). Suburban San Diego was under siege in October 2003 by the human-caused Cedar fire, which consumed an area unprecedented in California history (U.S. forest

Service, 2004). In 1988, 558,000 ha of the Greater Yellowstone Area in the western USA were torched by wildfires historic in intensity and community impact (Schullery, 1989). Fires in Greece in 2007 and 2009 were major news events; in 2009 the government faced strong criticism for the recurrence of death and destruction after just two years.

Global and regional warming trends have been identified and associated with exacerbated wildfire occurrence and impact (Stocks et al., 1998; Westerling et al., 2006). Attention to this topic has only been heightened with growing concern regarding anthropogenic climate forcing and fire's apparent increase in the wildland/urban interface. Attendant with that increased visibility is the need to better understand wildfire cause, behavior, dynamics, and linkage to climate.

Superimposed on this important topic is a relatively new discovery. Approximately ten years ago a new manifestation of extreme wildfire impact was identified: smoke in the stratosphere (Fromm et al., 2000). The cause is a particularly energetic form of blowup called pyrocumulonimbus (pyroCb for short). While pyroconvection and pyrocumulus have been well known for decades, the peculiar vertical extent of its impact potential escaped our

attention until 1998. In that year forest fires in northwestern Canada injected smoke (and certainly other related emissions) well beyond the tropopause; smoke was detected comfortably into the stratospheric "overworld[1]." This stratospheric penetration by cumulonimbus dynamics was in direct violation of the long-held meteorological assumption that thunderstorms penetrate—at best—marginally above the tropopause. The pyroCb has now been shown to effectively break through the tropopause's "lid" on convective vertical motion and deposit copious amounts of smoke that remains detectable for months (e.g. Fromm et al. 2008a,b).

Reports of confirmed pyroCb and stratospheric impact are increasing in the science literature, but the entire body of published cases accounts for fewer than ten events (Jost et al., 2004; Livesey et al., 2004; Damoah et al., 2006; Lindsey and Fromm, 2008; Cammas et al., 2009). However, since the advent of the "satellite era[2]" in 1979, several stratospheric mystery-layer events have been reported (e.g. Bluth, 1997; Clancy, 1986; Evans and Kerr, 1983). Moreover, one can find in the literature other cases wherein stratospheric aerosol layers are attributed to volcanic eruptions when no clear evidence of such an event exists (Yue et al., 1994). Similarly, there are scientific reports which describe stratospheric aerosol perturbations in the

aftermath of definitive volcanic injection into the stratosphere (e.g. Mount Pinatubo in 1991) wherein a subset of the aerosols do not conform to the eruption (Jäger, 1992; Trepte and Hitchman, 1992; Thomason, 1992). Finally, there exist published observations of aerosols or clouds in the lowermost stratosphere attributed to thin, sub-visual cirrus clouds (SVC) or ultra-thin tropopause cirrus (UTTC) in ambient conditions (e.g. relative humidity <100%) that may call into question the support for frozen particles (e.g. Nielson et al., 2007 and Peter et al., 2003). Might the pyroCb, still in its infancy of understanding, be a contributor to some of these phenomena? Now that the pyroCb has been characterized, does the evidence of such mysterious or challenging stratospheric observations allow us to reinterpret earlier assessments? More generally, can satellite-era data be exploited to go beyond case studies toward a pyroCb climatology? If so, a broad new understanding of the scale of wildfire activity, its relation to weather, and interaction with climate change is within reach.

Here we present a characterization of the seasonal occurrence of pyroconvection and pyroCb, and identify three individual cases in which the stratospheric impact of pyroCb has been missed or mis-identified. We employ nadir-viewing polar orbiter and geosynchronous satellite image data,

satellite-based profile data, in addition to ground-based lidar data in this pursuit. Using these resources we present evidence for a reinterpretation of selected stratospheric mystery-layer or volcanic aerosol reports in the literature.

PyroCb vs. Volcano

The canonical model of aerosol in the lower stratosphere (LS) is that the ultimate source (or pathway) for its material is the troposphere, and that material enters the LS by two primary irreversible mechanisms, slow cross-tropopause ascent in the tropics and rapid injection by volcanic eruptions (SPARC, 2006). While there is still uncertainty and active research regarding these and other mechanisms (e.g. Khaykin et al., 2009, Dessler et al., 2007, Wang, 2007), models of the lower and middle atmosphere do not take into account any other routine process for troposphere-to-stratosphere exchange.

Aerosols, being a basic atmospheric constituent, are a fundamental tracer of polluting processes that affect both the troposphere and stratosphere. Regarding the stratosphere, observational and model analyses

of aerosols are a basic means for understanding dynamics (e.g. Trepte and Hitchman, 1992), patterns and trends (e.g. Deshler, 2008). Since the discovery by Junge et al. (1961) of a stratospheric "background" of liquid sulfate particles, temporal and spatial changes to this "layer" have been well documented with the aid of space-based and groundbased profiling instruments (e.g. Jäger, 2005; Deshler et al., 2006; Hofmann, 1990; SPARC, 2006). One seasonal/regional stratospheric aerosol peculiarity that has also been extensively studied is the polar stratospheric cloud (PSC). These form generally inside the winter polar vortex and are caused by adiabatic and diabatic cooling of air masses leading to condensation and/or freezing (e.g. McCormick et al., 1981; Browell et al., 1990; Toon et al., 1990).

Decadal studies of stratospheric aerosol loading generally conform to the above-mentioned canonical model (Deshler, 2008), but many studies also acknowledge puzzling variations and "mystery clouds" of aerosols (e.g. Bluth, 1997). Moreover, a few relatively recent papers have reported on a provocative observation of cirrus-like thin layers just above the tropopause (Nielsen et al., 2007; Peter et al., 2003) Hence it seems our observations and interpretation of aerosol and cloud features in the LS are still evolving.

Three Mystery Seasons. In northern summers 1989 through 1991, puzzling LS aerosol features were observed from ground and space. Sassen and Horel (1990) reported on perplexing lidar signals (and eye-witness views) at Salt Lake City in August 1989. They concluded that the aerosols were volcanic in origin even though no confirmed volcanic eruption into the stratosphere occurred. The suspected volcano was Santiaguito in Guatemala, which indeed erupted on 19 July 1989, but did not inject material near the stratosphere according to an expert eyewitness (William Rose, personal communication, 2004). In summer 1990 there was an impressive and sudden increase in LS aerosol loading in the northern middle and high latitudes, according to Yue et al. (1994). They analyzed an entire season of Stratospheric Aerosol and Gas Experiment (SAGE) II aerosol profiles, which chronicled a weeks-long perturbation reaching an altitude of 17 km. Yue et al., in accordance with the canonical stratospheric model (and noting that every previous, similar observation of SAGE II aerosol perturbation had been associated with a reported volcanic eruption) searched unsuccessfully for a documented volcanic eruption in 1990, and hence concluded that the mystery cloud was attributable to an *unreported* volcanic eruption. In June 1991 Mount Pinatubo's cataclysmic eruption had a global,

multi-year impact (e.g. Hansen, 1996). Although this event was thoroughly observed and modeled, a perplexing occurrence of early LS aerosol layers in northern middle and high latitudes formed a sub-theme in papers on the resultant LS aerosol loading (e.g. Jäger, 1992; Gobbi et al., 1992; Trepte and Hitchman, 1992). Indeed there were sufficient SAGEII observations for Thomason (1992) to characterize a "new mode" of "Pinatubo aerosols" just above the tropopause in northern extratropics, peculiar in particle size (inferred by SAGE II wavelength dependence of extinction). In short, this class of aerosol was between the tropopause and roughly 16 km, and was smaller in diameter than the preponderance of Pinatubo aerosols higher and elsewhere globally.

Aerosol Index, The Unknown Smoke Signal. Soon after the discovery of stratospheric smoke in 1998, a signal of the immediate effect of violent pyroCb explosions began to take shape. The day after a pyroCb the absorbing aerosol index (AI) sensed by the Total Ozone Monitoring Spectrometer (TOMS) highlighted the smoke plume with peculiarly large AI values (e.g. Fromm et al., 2008a). AI is a positive number in the presence of absorbing aerosols such as dust, smoke, and ash. AI is strongly dependent on plume aerosol optical depth (AOD) and plume altitude (Torres et al.,

1998). At any given time on Earth there are optically opaque absorbing aerosol plumes. For example, in the burning season of Amazonia—perhaps the most familiar biomass burning region—smoke plumes are often expansive and optically opaque. Yet optically thick Amazonian smoke plumes have never had an AI > 12 in the TOMS satellite era (TOMS started operating in late 1978 and ended in 2005). In contrast, the "day after" pyroCb smoke plumes of events such as the Chisholm (Alberta) pyroCb of May 2001 (Fromm et al., 2008a) had AI> 20. In fact, some particularly extreme smoke plumes have fill/error values in the level 3 (i.e. gridded) AI where the level 2 (i.e. the instrument's native measurement footprint) AI manifests even greater intensity. Table 1 shows the ranking of AI in the TOMS era. A listing such as Table 1 is an invaluable tool for investigating causality. Quite simply it is a matter of looking at satellite image data and weather maps "upstream" one day for a phenomenon that might cause an optically thick, high altitude smoke plume. Thirteen of the top 20 AI plumes are smoke from documented or otherwise determined pyroCb events. The remaining events are also deep, thick, day-old smoke plumes that have not yet been definitively associated with their cause. Of these there are events in eastern Siberia wherein we suspect a substantial role played by a vigorous extratropical cyclone spinning up in the flaming zone. This type of

investigation, of these and other double-digit AI plumes, led us to a new interpretation of the 1989-1991 mystery cloud events.

Mystery Season 1: 1989. Fires in Manitoba and Saskatchewan in historically great number were ignited by lightning on 17 July 1989 (Hirsch, 1991). Four days later, on 21 July, extreme fire-weather conditions led to pyroconvection at a number of these fires, three of which spawned pyroCb. GOES imagery (not shown) pinpointed these blowups. Advanced Very High Resolution Radiometer (AVHRR) imagery (see Figure 1) captured the action in late afternoon. At least four pulses of deep pyrocumulonimbus anvils were in evidence. The "day after" AI plume on 22 July contained double-digit AI and plume-interior AI grid points with fill/error values suggesting a particularly extreme smoke pall.

Figure 1 shows the smoke plume evolution for the first week after the pyroCb. Evidently the smoke pall is sufficiently high and massive that it can be followed in AI across the Atlantic Ocean to Europe. We see also a part of the plume that advanced south across the USA, as far as Mexico, on 23 July. Remnants of this portion of the plume circulated in the southern USA and Central America. Fortuitously that part of the Canadian smoke plume was

sampled by SAGE II on 25 July; the profile is also part of Figure 1. The aerosol extinction profile exhibited a strong increase at 14 km altitude, and a wavelength dependence of extinction illustrative of particles with radius less than one micron. The back trajectory from this observation makes an excellent connection with the fire zone on 21-22 July. Hence we have an unambiguous confirmation of stratospheric smoke leading back to this pyroCb event in Canada. This is but one example of several similarly perturbed SAGE aerosol profiles that summer. Another fortuitous set of measurements of upper troposphere, lower stratosphere (UTLS) aerosols at that time was made in Manhattan Kansas (39.2ºN, 96.6ºW) by groundbased lidar during the First ISLSCP (International Satellite Land Surface Climatology Project) Field Experiment (FIFE) Follow-On project. The lidar (Eloranta, 2005) operated between late 26 July and 11 August, and on two occasions (26 July and 6 August) measured LS aerosol layers (http://lidar.ssec.wisc.edu/pub_html/fife/vil/1989/index.htm) that match up well via back trajectory with the pyroCb and the Sassen and Horel (1990) Salt Lake City observations, respectively.

Mystery Season 2: 1990. A discovery of pyroCb in 1990 was afforded by the large-AI "day-after" signal (Table 1). On 7 July 1990

AI=14.9 was located over far northern Alaska. A search through AVHRR imagery for that date revealed the classic "day-after" plume signature—an ashy gray cloud in visible bands, and very cold in thermal infrared (THIR) (Lindsey and Fromm, 2008). Moreover, the false-color image in Figure 2 shows fire hot spots in Alaska. We then examined GOES visible and THIR image loops for 6-7 July and isolated a pyroCb generated by a fire called the Circle Fire, located at 65.9ºN, 145ºW. Figure 2 shows the AI evolution in the week after the pyroCb. The plume drifts north and east over very high Arctic latitudes and then spreads over eastern Canada, the Maritimes, and Greenland. Like the 1989 plume, and others from documented pyroCb events (e.g. Fromm et al., 2005), this long-lived and transported AI signal represents abundant UTLS smoke aerosols.

Unlike the 1989 pyroCb event, there is no aerosol-layer measurement close enough in time to the pyroCb for trajectory matching analysis. However, Yue et al. (1994) described a large-scale SAGE II LS aerosol perturbation at mid and high northern latitudes in summer 1990. Here in Figure 2 we reanalyze the SAGE data in terms of daily (i.e. roughly zonal) average LS aerosol optical depth (AOD). In comparison with 1989, 1990 AOD was identical before the pyroCb but approached an approximate

doubling afterwards. A systematic increase in zonal average AOD was evident into November 1990, four months after the blowup. We conclude that the true source of this hemispheric LS aerosol increase was the Circle Fire pyroCb on 6 July, not a volcanic eruption. Moreover, a doubling of zonal average LS AOD is qualitatively equivalent to the perturbation caused by the Canberra and Chisholm pyroCbs (Fromm et al., 2006, 2008).

Mystery Season 3: 1991. Eighth on the list of greatest AI in Table 1 is a smoke plume on 21 June 1991. This plume was located over the Atlantic Ocean northwest of the Iberian peninsula. One day prior there was also a large-AI plume over Newfoundland. On 19 June there were two pyroCbs in Québec, one of which was evidently mature in Figure 3. Two separate fires spawned the pyroCbs, one near Baie Comeau (the site of the largest/brightest hot spot in Fig. 3). Figure 3 shows the AI evolution of smoke as the plume rapidly crossed the Atlantic and reached Russia within a week of the blowup. On 22 June the core of the AI plume was situated over northern Europe near Denmark. On that day SAGE II made a measurement slightly east of Denmark (Figure 3) that contained a huge aerosol enhancement two km above the tropopause. Indeed this SAGE measurement was the source of a high-AOD feature on a global AOD map

illustrating the cover of Geophysical Research Letters of 24 January 1992—an issue partly dedicated to first Pinatubo results. The trajectory from the 22 June SAGE layer implicates the Québec pyroCbs, not Mt. Pinatubo.

In addition to the SAGE measurements, a number of lidar measurements made in the weeks after the Pinatubo eruption also detected LS aerosols that were difficult to reconcile with the suggestion that they could have been produced by the volcano. Figure 4 shows that on 1 July 1991 lidars in Germany, France, and Italy all detected layers at 15-16 km, and whose back trajectories (not shown) seemingly rule out a path from Pinatubo by virtue of a common westerly flow leading back across North America and remaining in midlatitudes through mid-June. Figure 5 shows a time series of the 313-nm backscatter coefficient recently calculated from measurements with the ozone lidar (Carnuth et al., 2002) at Garmisch-Partenkirchen, Germany on 1-3 July 1991. These data reveal very high backscatter coefficients in the lower stratosphere between 13 and 16 km during two specific periods, but much less in the evening of July 1 when the 532-nm measurements in Figure 4 were made. The peak backscatter coefficient reached 8×10^{-6} m^{-1} sr^{-1}. We calculated 111 315-h HYbrid Single-Particle Lagrangian Integrated Trajectory (HYSPLIT) backward

trajectories (for this episode every three hours, starting at altitudes between 13.5 and 16 km over Garmisch-Partenkirchen. Trajectories from the two relatively strong plumes closely overpass the region around Québec City (not shown). All the trajectory paths can be generally characterized as westerly; endpoints (between 17 and 19 June) ranged from the western Atlantic Ocean through Central and North America to the eastern Pacific Ocean. The characteristic path of air reaching these three lidar sites is thus entirely inconsistent with the Mt. Pinatubo plume, the movement of which was strictly easterly from the eruption, and constrained with 20° latitude of the Equator (Bluth et al., 1992).

Thus it appears that the pyroCb mechanism offers a reinterpretation for part of the widespread aerosol pollution of the northern LS in the summer of 1991, as well as the mystery clouds in 1989 and 1990.

How Frequent Are PyroCbs?

The lesson of the prior discussion includes a realization that pyroCb occurrence is both greater than expected and an unknown contributor to historical smoke-plume events. It is also reasonable to conclude that, like

"regular" cumulonimbus, pyrocumulonimbus vary in intensity from the relatively rare, deepest stratospheric polluters to more frequent storms of lesser vertical extent. We explore these issues here, where we focus on one season—2002—in North America. Much of southwestern USA experienced particularly intense drought in 2002 (Quiring and Goodrich, 2008). During that season, a Canadian pyroCb was shown to be the source for in situ measurements of biomass burning tracers in the LS (Jost et al., 2004). However, Jost et al. also came to the conclusion that deep pyroconvective activity was also likely to have occurred in the western USA that summer. Partly aided by the TOMS AI record, we surveyed the period May-September 2002 for other UTLS smoke plumes and pyroconvection.

Fire Season 2002. Figure 6, what we term the "Smoke Seismograph," shows how daily AI extremes for a fixed geographic area vary with time. Interpreting the spikes as a signal of a particularly intense and high smoke plume, we identify candidate events to explore more deeply. Note that the spikes of interest need not be double-digit values of the historically greatest plumes of Table 1; any sharp day-to-day AI increase is a clue to a story worth exploring. It is of course also expected that some noteworthy plumes may be "hidden" among other more intense AI signals

over an area as large as used for Figure 6. Hence the Smoke Seismograph probably under-represents pyroconvective plumes. We investigated the AI spike events (AI>5) by noting the date/coordinates of the plume, examining GOES imagery "upstream" on the prior date, and searching fire databases to confirm fire location. For USA fires we used a compilation of Incident Status Summary ICS-209 reports maintained by the US Forest Service (Charles McHugh, personal communication, 2009). For Canada we used the Large Fire Database (LFDB) (Stocks et al., 2002). Pyrocumulus (pyroCu) convection is considered to have occurred if the short-wavelength infrared (SWIR, 3.9μm) GOES imagery contains fire hot spots and THIR imagery shows cloud, anchored to the hot spots, with colder-than-land brightness temperature (BT)—"dry" smoke plumes are transparent to THIR radiation. The pyroCb, a subclass of pyroCu, is indicated when the fire-anchored cloud pixels have BT < -40ºC. The likelihood of pyroCb detection is increased by using the SWIR image of the fire-anchored cold (in THIR) cloud, which in daylight conditions will emit as an anomalously high BT owing to the peculiarly small particle size within smoky pyroCb anvils (Lindsey and Fromm, 2008).

Pyroconvection in 2002. Table 2 gives a listing of the 2002 pyroCbs and "smoking gun" fires discovered by this method. Figure 7 is a map of fires > 200 ha, pyroCu, and pyroCb, which are also annotated by date on the Smoke Seismograph. The Smoke Seismograph shows that from 1-25 May, daily maximum AI was relatively low and invariant. Except for isolated spikes, AI at the end of the 2002 fire season was similarly invariant, and decreasing--consistent with light/declining wildfire activity. However, starting on 26 May AI-spike frequency increases strongly and remains the dominant feature through July. On nine days between June and August, maximum AI reaches double digit values. The first spike in May is attributable to a complex of fires and pyroconvection in eastern Alberta. Here the pyroCu cloud tops reached (GOES) BT of -22ºC, which according to the nearest radiosonde gives height/pressure of 5.9 km/470 hPa. More pyroCu were detected in Alberta on 31 May with upper tropospheric cloud-top heights. Between 2 June and 28 July we identified 16 pyroCbs, 9 in the two-week period 18 June – 1 July. Noteworthy among these are the Hayman Fire in Colorado, which erupted into pyroCb within one day of ignition, a second time on 18 June, and the Rodeo-Chediski fire complex in Arizona. These were the two largest fires in the history of these two states and both were anthropogenic (Graham, 2003; Ffolliott et al., 2008). On one

occasion, 2 June, pyroconvection and two pyroCbs erupted from three separate fires along the Colorado/New Mexico border. One of these fires (named "Unknown") was not included in the US Forest Service fire database. On four consecutive days between 18 and 21 June, pyroCbs exploded in Arizona, Colorado, and Alberta. On three consecutive days in mid-July pyroCbs were found in Colorado and Oregon. Two of these were generated by a single fire, the Burn Canyon Fire, roughly 24 hours apart.

Pyrocumulonimbus storms are an obviously extreme form of convection, yet they occurred in 2002 in environmental conditions far from typical for severe convection. Table 2 contains two stability measures, Convective Available Potential Energy (CAPE), and the Lower Atmospheric Severity Index (LASI) for wildland fires, better known as the Haines Index (Haines, 1988). There is no single CAPE threshold for severe convection, however it is usually associated with values exceeding 2500 J/kg, which implies a conditionally unstable lapse rate combined with abundant lower tropospheric water vapor. In contrast the Haines Index, which also includes a lapse-rate and moisture term, signals extreme fire behavior only when an unstable lapse rate is matched with a dry lower troposphere. In the case of the 17 pyroCbs in Table 2, CAPE conditions were consistently slight.

Indeed in roughly half of the pyroCb events there was zero CAPE. However, the Haines Index registered its maximum value of 6 (indicating conditions for high rate of fire spread) for all of the pyroCbs in the USA and one in Canada. Of the remaining Canadian pyroCbs, all but one had a Haines Index of 5. Thus it is apparent that the fundamental predictor for pyroCb occurrence must take into account factors other than those for severe "regular" convection.

Perhaps fire size is an important metric for predicting pyroCb. Table 2 lists the final fire size for the "smoking guns." They were all large fires but the final burned-area perimeter varies by two orders of magnitude. We did not have access to time-resolved fire-size change for Canada fires; this would be a critical value to have to associate fuel consumed on the days of pyroconvection versus the other days in the fire's lifetime.

Stratospheric smoke in 2002. In addition to the stratospheric impact Jost et al. (2004) reported from Canadian fires (on 27 June), there is strong evidence of stratospheric smoke from three additional pyroCbs--Hayman (9 June), a pyroCb ensemble between 18-20 June in Colorado/Arizona, and the Mustang pyroCb on 1 July (David Knapp et al., in preparation, 2009). The

evidence is from satellite and ground-based aerosol profiles. For instance on 21 June, the Purple Crow lidar (Sica et al., 1995) in London, Ontario, 42.9ºN, 81.4ºW, detected an aerosol layer between 11.6 and 14.5 km altitude, straddling the tropopause at 13.3 km (Figure 8). An isentropic back trajectory passes over Colorado close to the Hayman fire on 18 June, the site of a second pyroCb from this fire (Table 2). This supports Jost et al.'s contention regarding additional occurrences of deep pyroconvection--impacting the UTLS--in 2002.

PyroCb Injection Altitude. It is abundantly evident, considering the published reports of stratospheric pollution by pyroCb, that the effective maximum height of a pyroCb's emissions is at or above the convective cloud top altitude. A conventional method by which to infer cloud-top height (for optically opaque clouds such as thunderstorm anvils) is by way of cloud-top thermal infrared brightness temperature matched against the environmental lapse rate (Smith and Platt, 1978). Even though this method entails uncertainty for clouds in the tropopause region owing to potential non-singularity in the temperature/height profile, it can still provide a confident—albeit conservative—value for outflow height. We employed

this method for the events in Table 2. The average pyroCb emission-altitude/pressure extreme here is 11.7 km/220 hPa.

Diurnal pyroCb behavior. It is essential to characterize a typical day in the life of a pyroCb, not only to understand the fire and fire-storm behavior, but to also to characterize the time-change of emission height. This knowledge will inform fire behavior analysts, users of satellite data, and modelers. Since the discovery of pyroCb, they have been observed by satellite to occur in morning, afternoon, and in middle-night hours. Even in 2002, among the 16 pyroCb events, one occurred at approximately 11 am local (the Meadow fire pyroCb on 24 June), and one occurred near local midnight (Burn Canyon, on 13 July). However, the preponderance or pyroCbs reached maturity in late afternoon, around 6 pm local time (Table 2). We have analyzed all 16 in terms of local time, using GOES IR imagery to identify fire growth, pyrocumulus onset, and maturity. Here we centered each fire in a grid of GOES pixels approximately 48 km on a side and recorded certain metrics at each image time, e.g. the maximum 11um BT (BTmax) and minimum 11um BT (BTmin). The Btmin metric is with respect to radiosonde-derived Lifted Condensation Level (LCL) temperature. Negative values suggest pyrocloud formation; the more negative the value the higher the pyrocloud. Fire hot spot size change is

tracked with 3.9 um BT. A qualitative index is formed by counting hot spot pixels and dividing by the maximum for that fire/pyroCb.

Figure 9 is a presentation of the average over all 16 pyroCb events. The fire-size metric shows that before local noon, fire size is negligible, consistent with the general diurnal behavior of tropical and subtropical wild fire (Giglio, 2007). Toward midday fire size increases and peaks in early afternoon. Undoubtedly this metric is impacted by cloud formation and is thus not solely influenced by fire behavior. However, in the mean it is apparent these fires that erupted into pyroCb spent the first half of the day relatively inactive.

The BTmax trace, which likely represents clear-sky pixels, shows morning warming and a peak around 1 pm. The BTmin curve generally follows BTmax until 1100 LT, when it peaks and begins a steep decline. This signifies the onset of pyroconvection wherein cloud formation in the flaming area begins to modify the diurnal clear-sky radiance progression. At roughly 1330 LT BTmin goes negative, indicating effectively that an optically thick pyrocumulus cloud fills a GOES 4km^2 pixel. Thus at this point the emissions from the fire may be assumed to reach as high as the

LCL, which on average here is 4.1 km (632 hPa). From this point pyroconvection intensifies steadily (in the average sense) until a peak at roughly 6 pm local, when the pyroCb can be considered in full maturity. At this point the pyroCb is exhausting a considerable amount of biomass burning emissions in the UTLS.

Thus in the typical diurnal cycle of fire behavior that includes pyrocumulonimbus energy it can be expected that exhaust from this fire will span the troposphere in the course of a day. It is reasonable then to conclude that a considerable proportion of the emissions—during the hours of deepest pyroconvection—will be injected into the uppermost troposphere, above precipitation/scavenging processes. This is indeed a fundamental reinterpretation of fire vertical injection potential that is not well characterized in regional or global atmospheric models of chemistry and transport.

Summation

Since the discovery of smoke in the stratosphere and pyroCb only a small number of individual case studies and modeling experiments (Trentmann et al. 2006; Luderer et al., 2006; Cunningham and Reeder, 2009) have been performed. Hence there is still much to be learned about pyroCb and its importance. With this work we have attempted to reduce the unknowns by revealing several additional occasions when pyroCbs were either a significant or sole cause for the type of stratospheric pollution usually attributed to volcanic injections. Now it is established that pyroCb activity is sufficiently frequent that a measurable stratospheric increase in aerosols attributable to this process occurred in 1989-1991, 1992 (Livesey et al. 2004), 1998 (Fromm et al., 2000, 2005), 2001-2004 (Fromm et al., 2003, 2006, 2008a,b; Cammas et al., 2009). Unpublished analyses of satellite data (e.g. SAGE II aerosol profiles and imager data) have also revealed pyroCbs and stratospheric aerosol layers attributable to the Great China Fire in May 1987 (Cahoon et al., 1994) and the Yellowstone fires of 1988 (Schullery, 1989). Hence it can be concluded that for six consecutive years (1987-1992) the pyroCb phenomenon was routine and its stratospheric impact identifiable. As research continues, stratospheric impact by pyroCb will be further refined.

On an intra-seasonal level we have established that pyroCb occur with surprising abundance. In 2002, at least 17 pyroCbs erupted in North America alone. Still to be determined is how often this process occurred in the boreal forests of Asia in 2002. However, it is now established that this most extreme form of pyroconvection—along with more frequent pyrocumulus convection—was widespread and persisted for at least two months. The characteristic injection height of pyroCb emissions is the upper troposphere; a subset of these storms pollutes the lower stratosphere. Thus a new appreciation for the role of extreme wild-fire behavior and its atmospheric ramifications are now coming into focus.

Considering these now-told stories of pyroCb behavior, it is quite likely that future blowups will permit continued study of these events as they unfold. Satellite imagery and data such as those shown herein are indispensable for such analyses. We consider it very important to note the continued need for global monitoring by nadir viewing imagers and stratospheric monitoring by instruments such as NASA's Cloud-Aerosol Lidar and Infrared Pathfinder Satellite Observation (CALIPSO) (e.g. Thomason et al., 2007). Satellite data were the true source for the discovery

of pyroCbs and smoke in the stratosphere; their value toward future studies and discoveries is inestimable.

Footnotes

_1. "Overworld," A term coined by James Holton, is the range of stratospheric altitudes roughly greater than the 380 K potential temperature surface. This threshold generally defines that absolute top of the tropopause region anywhere on the globe.

_2. The "satellite era" for our purposes is defined as beginning in 1979, when polar orbiting weather satellites with imaging and Earth radiation budget instruments, and other instruments such as NASA's Total Ozone Mapping Spectrometer (TOMS), and a host of solar occultation devices went into service.

Table 1. Total Ozone Mapping Spectrometer (TOMS) Aerosol Index (AI) Greatest Value Ranking. Events listed in descending order of AI.

AI	Plume Date	Lat.(°) +N,-S	Lon.(°) +E,-W	Cause	Source Location	Notes
29.9	29 May	65	-112	pyroCb	Alberta	Chisholm

	2001				Canada	Fire; Fromm and Servranckx, (2003)
25.9	19 Jan 2003	-32	163	pyroCb	Canberra Australia	Pyro-tornado; Cunningham and Reeder (2009)
25.3	5 Aug 1998	73	-64	pyroCb	Northwest Territories Canada	Norman Wells pyroCb; Fromm et al. (2005)
18.8	18 Aug 2003	61	-89	pyroCb	Northwest Territories Canada	Conibear Lake Fire; Wood Buffalo National Park

17.9	27 Aug 2000	42	-92	pyroCb	South Dakota USA	Jasper Fire; Black Hills National Forest
16.5	27 Sep 1998	69	148	TBD	Khabarovsk Russia	
16.2	18 Dec 2002	-35	144	pyroCb	Victoria Australia	Big Desert Wilderness Park
15.9	21 Jun 1991	45	-24	pyroCb	Quebec Canada	Baie-Comeau Fire (discussed in this paper)
15.6	4 May 2003	57	153	TBD	Eastern Russia	
15.6	10 Jun 2002	45	-101	pyroCb	Colorado USA	Hayman Fire
15.4	10 Sep	46	-89	pyroCb	Wyoming	Yellowstone

	1988				USA	National Park
14.9	7 July 1990	70	-152	pyroCb	Alaska USA	Circle Fire
14.9	8 May 1987	62	133	TBD	Northern Mongolia	Great China Fire; Cahoon et al. (1994)
14.4	23 Aug 1998	49	153	TBD	Khabarovsk Russia	
14.3	27 Jan 2003	-39	168	TBD	Southeastern Australia	
14.3	20 Jun 2002	39	-104	pyroCb	Arizona USA	Rodeo-Chediski Fire
14.1	19 Jun 2002	42	-99	pyroCb	Colorado USA	Hayman Fire
14.0	6 May 2003	48	142	TBD	Eastern Russia	

14.0	1 Feb 2003	-28	-178	TBD	Southeastern Australia	
14.0	19 Aug 2000	48	-107	pyroCb	Idaho USA	

Table 2. PyroCbs in USA and Canada, 2002.

Name (Final size, ha)	Date	Lat (N)	Lon (W)	BTmin (C)	Cloudtop z/p (km/hPa)	LCL z./p (km/hPa)	Haines Index/ CAPE (J/kg)	RAOB Site
Spring (6,677)	2 June	37.0	105.0	-43.0	10.4/267	5.2/544	6/583	ABQ
Unknown	2 June	37.0	104.4	-52.0	10.4/267	5.2/544	6/583	ABQ
Hayman (55,749)	9 June	39.2	105.4	-56.1	12.3/200	6.1/483	6/92	DNR
Hayman (55,749)	17 Jun	39.2	105.4	-56.2	11.6/222	4.9/561	6/918	DNR
Hayman (55,749)	18 June	39.1	105.3	-53.1	11.5/225	6.3/490	6/0	DNR
Million	19	37.7	106.7	-58.0	12.2/200	5.5/519	6/287	GJT

(3,782)	June							
Rodeo/Chediski (189,651)	20 June	34.2	110.5	-44.1	10.2/270	5.1/559	6/0	FGZ
Dobbin (151,640)	21 June	56.7	104.5	-58.1*	11.8/207	2.5/760	6/135	YQD
Meadow (75,483)	24 June	56.8	108.5	-44.1	9.5/290	2.2/782	5/0	YSM
Lobb (62,171)	27 June	55.3	103.3	-58.0	12.4/187	2.5/762	5/0	YQD
Nagle (71,029)	27 June	56.2	105.1	-61.0	12.8/182	2.5/762	5/0	YQD
56N109W	27 June	56.5	108.8	-58.0*	12.2/197	1.7/819	4/11	YSM
Mustang (8,109)	1 July	41.0	109.3	-60.0	13.0/184	4.1/623	6/18	SLC
Burn Canyon (12,667)	13 July	38.0	108.4	-53.1	11.9/216	6.0/494	6/768	GJT
Burn Canyon (12,667)	14 July	38.0	108.4	-53.1	12.6/193	5.5/532	6/420	GJT
Winter (14,479)	15 July	42.8	120.8	-43.1	10.7/258	3.6/672	6/0	BOI
Florence/Biscuit (202,169)	28 July	42.3	123.9	-50.2	11.6/232	2.4/770	6/0	MFR

Average					11.6/223	4.19/628.0		

* BTmin < RAOB Tmin

Figure Captions

Figure 1. Composite of AVHRR, aerosol index (AI), SAGE layer, and trajectory for 1989 Manitoba and Saskatchewan pyroCbs. (a) AVHRR false-color rendering of 3.7, 0.86, and 0.63μm radiance for local evening 21 July 1989. (b) SAGE II aerosol extinction profile. (c) Map of TOMS AI color coded by date, between 22 and 27 July 1989, location of pyroconvection (+), the SAGE profile location (white dot), and trajectory (blue line) at SAGE-layer altitude ending 00 UTC 22 July.

Figure 2. Composite of AVHRR, AI, and SAGE AOD for 1990 Circle pyroCb. (a) AVHRR 11 μm brightness temperature and 0.63μm reflectance image for local evening 6 July 1990 over northern Alaska. IR color enhancement shows BT < -40°C. (b) SAGE II measurement-latitude pattern for 1989 and 1990 (top) and daily average LS AOD (bottom) for June through December. (c) Map of TOMS AI color coded by date, between 7 and 12 July 1990 and location of pyroconvection (+).

Figure 3. Composite of AVHRR, AI, SAGE layer, and trajectory, for 1991 Quebec pyroCbs. (a) AVHRR false-color rendering of 3.7, 0.86, and

0.63μm radiance for local evening 19 June 1991. (b) SAGE II aerosol extinction profile. (c) Map of TOMS AI color coded by date, between 20 and 25 June 1991, location of pyroconvection (+), and trajectory (blue line) at SAGE-layer altitude ending 00 UTC 20 June.

Figure 4. Three European lidar layers in July 1991(a) and isentropic back trajectories (b). Entire trajectory ends on 15 June. Colored segment ends ~12 UTC 26 June 1991.

Figure 5. Color-coded time series of the 313-nm backscatter coefficient derived from lidar measurements at Garmisch-Partenkirchen on 1-3 July 1991; the time is given in Central European Time (= UTC + 1 h). Tropopause height from Munich radiosondes annotated as black horizontal line segments over "TP." White-out areas indicate no measurements (22-29 CET) or measurements not possible (e.g. due to clouds).

Figure 6. Smoke Seismograph for 2002. Daily maximum NASA TOMS aerosol index over North America, May-October. Annotations for dates of pyroCu and pyroCb.

Figure 7. Map of 2002 pyroCu (green diamonds), pyroCb (red filled circles), and Canada/USA fires > 200 ha (white dots).

Figure 8. Purple Crow lidar aerosol backscatter, 21 June 2002 and Buffalo radiosonde temperature profile, 21 June 00 UTC. Back trajectory superimposed on AI map like Figures 1-3. Back trajectory altitude is 13 km and endpoint is 19 June, 00 UTC.

Figure 9. Average diurnal cycle for fire and pyrocloud for 16 pyroCb events in 2002. See text for pixel box used. Hot spot index is a count of hot spot pixels relative to the maximum observed (dotted line). 11um BT maximum in the box (dashed line); 11um BTmin-LCL temperature (solid black line).

References

Bluth, G.J.S., S. Doiron, C. Schnetzler, A. Krueger, and L. Walter (1992), Global tracking of the SO2 clouds from the June, 1991 Mount Pinatubo Eruptions, *Geophys. Res. Lett.*, **19**, 151-154.

Bluth, G.J.S., W.I. Rose, I.E. Sprod and A.J. Krueger (1997). Stratospheric loading from explosive volcanic eruptions, *Journ. of Geology*, **105**, 671-683.

Browell, E. V., C. F. Butler, S. Ismail, P. A. Robinette, A. F. Carter, N. S. Higdon, O. B. Toon, M. R. Schoeberl, and A. F. Tuck (1990), Airborne lidar observations in the wintertime Arctic stratosphere: Polar stratospheric clouds, *Geophys. Res. Lett.*, 17(4), 385–388.

Cahoon, D. R., B. J. Stocks, J. S. Levine, W. R. Cofer, J. M. Pierson (1994), Satallite analysis of the severe 1987 forest fires in northern China and southeastern Siberia, *J. Geophys. Res.*, **99**, 18627-18638.

Cammas, J.-P., J. Brioude, J.-P. Chaboureau, J. Duron, C. Mari, P. Mascart, P. Nédélec, H. Smit, H.-W. Pätz, A. Volz-Thomas, A. Stohl, and

M. Fromm (2009), Injection in the lower stratosphere of biomass fire emissions followed by long-range transport: a MOZAIC case study, *Atmos. Chem. Phys.*, **9**, 5829-5846.

Carnuth, W., U. Kempfer, T. Trickl (2002), Highlights of the Tropospheric Lidar Studies at IFU within the TOR Project, Tellus B, **54**, 163-185.

Clancy, R. T. (1986), El Chichon and "mystery cloud" aerosols between 30 and 55 km: Global observations from the SME visible spectrometer, *Geophys. Res. Lett.*, **13**(9), 937–940.

Cunningham P., M. J. Reeder (2009), Severe convective storms initiated by intense wildfires: Numerical simulations of pyro-convection and pyro-tornadogenesis, *Geophys. Res. Lett*., **36**, L12812, doi:10.1029/2009GL039262.

Damoah, R., N. Spichtinger, R. Servranckx, M. Fromm, E. Eloranta, I. Razenkov, P. James, M. Shulski, C. Forster, and A. Stohl (2006), A case study of pyro-convection using transport model and remote sensing data, *Atmos. Chem. Phys.*, 6, 173-185.

Deshler, T., R. Anderson-Sprecher, H. Jäger, J. Barnes, D. J. Hofmann, B. Clemesha, D. Simonich, M. Osborn, R. G. Grainger, S. Godin-Beekmann (2006), Trends in the nonvolcanic component of stratospheric aerosol over the period 1971–2004. *J. Geophys. Res.* **111**, D01201. doi:10.1029/2005JD006089.

Deshler, T. (2008), A Review of Global Stratospheric Aerosol: measurements, importance, life cycle, and local stratospheric aerosol, *Atmos. Res*., **90**, 223-232.

Dessler, A.E., T. F. Hanisco, and S. Fueglistaler (2007) Effects of convective ice lofting on H2O and HDO in the tropical tropopause layer, *J. Geophys. Res.* 112, D18309, DOI: 10.1029/2007JD008609.

Eloranta, E. W. (2005), High Spectral Resolution Lidar, Lidar: Range-Resolved Optical Remote Sensing of the Atmosphere, edited by: Weitkamp, K., Springer Series in Optical Sciences, Springer Verlag, New York, USA, 143–163, 2005

Ffolliott, Peter F.; Stropki, Cody L.; Neary, Daniel G (2008), Historical wildfire impacts on ponderosa pine tree overstories: An Arizona case Study, Res. Pap. RMRS-RP-75, Fort Collins, CO: U.S. Department of Agriculture, Forest Service, Rocky Mountain Research Station, 24 p.

Fromm, M., Alfred, J., Hoppel, K., Hornstein, J., Bevilacqua, R., Shettle, E., Servranckx, R., Li, Z., and Stocks, B. Observations of boreal forest fire smoke in the stratosphere by POAM III, SAGE II, and lidar in 1998. *Geophys. Res. Lett*. 27, 1407-1410 (2000).

Fromm, M., and Servranckx, R. Transport of forest fire smoke above the tropopause by supercell convection. *Geophys. Res. Lett*. **30**, doi: 10.1029/2002GL016820 (2003).

Fromm, M. Bevilacqua, R., Servranckx, R., Rosen, J., Thayer, J., Herman, J., and Larko, D. Pyro-cumulonimbus injection of smoke to the stratosphere: Observations and impact of a super blowup in northwestern Canada on 3-4 August 1998. *J. Geophys. Res.* **110**, doi: 10.1029/2004JD005350 (2005).

Fromm, M., Torres, O., Diner, D., Lindsey, D., Vant Hull, B., Servranckx, R., Shettle, E., Li, Z., The stratospheric impact of the Chisholm PyroCumulonimbus eruption: 1. Earth-viewing satellite perspective. *J. Geophys. Res*. **113**, D08202, doi:10.1029/2007JD009153 (2008).

Fromm, M., Shettle, E., Fricke, K. H., Ritter, C., Trickl, T., Giehl, H., Gerding, M., Barnes, J., O'Neill, M., Massie, S., Blum, U., McDermid, I., Leblanc, T., Deshler, T., The stratospheric impact of the Chisholm PyroCumulonimbus eruption: Part II, vertical profile perspective. *J. Geophys. Res*. **113**, D08203, doi:10.1029/2007JD009147 (2008).

Fromm M., Tupper, A., Rosenfeld, D., Servranckx, R., McRae, R. Violent pyro-convective storm devastates Australia's capital and pollutes the stratosphere, *Geophys. Res. Lett.* **33**, L05815, doi:10.1029/2005GL025161 (2006).

Giglio, L. (2007), Characterization of the tropical diurnal fire cycle using VIRS and MODIS observations, *Remote Sens. of Environ*., 108, 407-421.

Gobbi, G. P., F. Congeduti, and A. Adriani (1992), Early stratospheric effects of the Pinatubo eruption, *Geophys. Res. Lett*., 19(10), 997-1000.

Graham, Russell T., Technical Editor (2003), Hayman Fire Case Study, Gen. Tech. Rep. RMRS-GTR-114. Ogden, UT: U.S. Department of Agriculture, Forest Service, Rocky Mountain Research Station, 396 p.

Haines, D. A. (1988), A lower atmospheric severity index for wildland fire, *Natl. Wea. Dig*., 13, 23-27.

Hansen, J., R. Ruedy, M. Sato, and R. Reynolds (1996), Global surface air temperature in 1995: Return to pre-Pinatubo level, *Geophys. Res. Lett.*, 23(13), 1665–1668.

Hirsch, K.G. (1991), A chronological overview of the 1989 fire season in Manitoba, *Forestry Chronicle*, 67 (4), 358-365.

Hofmann, D.J. (1990), Increase in the stratospheric background sulfuric acid aerosol mass in the past 10 years, *Science*, **248**, 996–1000.

Jäger, H. (1992), The Pinatubo eruption cloud observed by lidar at Garmisch Partenkirchen, Geophys. *Res. Lett.*, 19(2), 191-194.

Jäger, H., 2005. Long-term record of lidar observations of the stratospheric aerosol layer at Garmisch-Partenkirchen. *J. Geophys. Res*. **110**, D08106. doi:10.1029/2004JD005506.

Jost, H., Drdla, K., Stohl, A., Pfister, L., Loewenstein, M., Lopez, J., Hudson, P., Murphy, D., Cziczo, D., Fromm, M., Bui, T., Dean-Day, J., Mahoney, M., Richard, E., Spichtinger, N., Vellovic, J., Weinstock, E., Wilson, J., Wofsy, S. In-situ observations of mid-latitude forest fire plumes deep in the stratosphere. *Geophys. Res. Lett*. **31**, doi:10.1029/2003GL019253 (2004).

Junge, C.E., C.W. Chagnon, and J.E. Manson (1961), Stratospheric aerosols. *J. Atmos. Sci.*, **18**, 81–108.

Khaykin, S., J.-P. Pommereau, L. Korshunov, V. Yushkov, J. Nielsen, N. Larsen, T. Christensen, A. Garnier, A. Lukyanov, and E.Williams, (2009) Hydration of the lower stratosphere by ice crystal geysers over land convective systems, Atmos. Chem. Phys., 9, 2275–2287.

Lindsey, D. T. and M. Fromm (2008), Evidence of the cloud lifetime effect from wildfire-induced thunderstorms, *Geophys. Res. Lett.*, 35, 22, L22809.

Livesey, N., Fromm, M., Waters, J., Manney, G., Santee, M., and Read, W. Enhancements in lower stratospheric CH_3CN observed by UARS MLS following boreal forest fires. *J. Geophys. Res*. **109,** D06308, doi:10.1029/2003JD004055 (2004).

Luderer, G., J. Trentmann, T. Winterrath, C. Textor, M. Herzog, H. F. Graf, M. O. Andreae (2006), Modeling of biomass smoke injection into the lower stratosphere by a large forest fire (Part II): sensitivity studies, *Atmos. Chem. Phys.*, 6, 5261-5277.

McCormick, M.P., et al. (1981), High-latitude stratospheric aerosols measured by the SAM II satellite system in 1978 and 1979, *Science*, **214**, 328–331.

Nielsen, J. K., N. Larsen, F. Cairo, G. Di Donfrancesco, J. M. Rosen, G. Durry, G. Held, and J.-P. Pommereau (2007), Solid particles in the tropical lowest stratosphere, Atmos. Chem. Phys., 7, 685–

695.

Peter, T., et al. (2003), Ultrathin Tropical Tropopause Clouds (UTTCs): I. Cloud morphology and occurrence, *Atmos. Chem. Phys*., **3**, 1083–1091.

Quiring, S. M. and G. B. Goodrich (2008), Nature and causes of the 2002-2004 drought in the southwestern United States compared with the historic 1953-19657 drought, *Clim. Res.*, 36 (1), 41-52.

Sassen, K., and J. Horel (1990), Polarization lidar and synoptic analyses of an unusual volcanic aerosol cloud, *J. Atmos. Sciences*, 47 (24), 2881-2889.

Schullery, P. (1989), Yellowstone fires: a preliminary report, *Northwest Science,* 63 (1), 44–54.

Sica, R. J., Sargoytchev, S., Argall, P. S., Borra, E. F., Girard, L., Sparrow, C. T., and Flatt, S. (1995), Lidar measurements taken with a large-aperture liquid mirror. 1. Rayleigh-scatter system, *Appl. Optics*, 34, 6925-6936.

Smith, W. L. and C. M. Platt, (1978), Comparison of satellite-deduced cloud heights with indications from radiosonde and ground-based laser measurements, *J. Appl. Meteorol*., 17, 1796-1802.

SPARC (2006), Assessment of Stratospheric Aerosol Properties, L. Thomason and Th. Peter , Ed., WCRP-124, WMO/TD- No. 1295, SPARC Report No. 4.

Stocks, B., Fosberg, M., Lynham, T., Mearns, L., Wotton, B., Yang, Q., Jin, J-Z., Lawrence, K., Hartley, G., Mason, J., and McKenney, D. (1998), Climate change and forest fire potential in Russian and Canadian boreal forests. *Climatic Change* **38(1)**, 1-13.

Stocks, B.J.; J. A. Mason, J. B. Todd, E. M. Bosch, B. M. Wotton, B. D. Amiro, M. D. Flannigan, K. G. Hirsch, K. A. Logan, D. L. Martell, W. R. Skinner (2002), Large forest fires in Canada, 1959–1997, *J. Geophys. Res*. 107,8149,doi:10.1029/2001 JD000484.

Thomason, L. (1992), Observations of a new SAGE II aerosol extinction mode following the eruption of Mt. Pinatubo, *Geophys. Res. Lett.*, 19(21), 2179-2182.

Thomason, L.W., L. R. Poole, and T. Deshler (1997), A global climatology of stratospheric aerosol surface area density deduced from stratospheric aerosol and gas experiment II measurements: 1984–1994, J. *Geophys. Res.* **102**, 8967–8976.

Thomason, L. W., Pitts, M. C., and Winker, D. M. (2007), CALIPSO observations of stratospheric aerosols: a preliminary assessment, Atmos. Chem. Phys., 7, 5283-5290.

Toon, O. B., E. V. Browell, S. Kinne, and J. Jordan (1990), An analysis of lidar observations of polar stratospheric clouds, *Geophys. Res. Lett.*, **17(4)**, 393–396.

Torres, O., P. K. Bhartia, J. R. Herman, Z. Ahmad, J. Gleason (1998), Derivation of aerosol properties from satellite measurements of

backscattered ultraviolet radiation: Theoretical basis, *J. Geophys. Res.*, 103(D14), 17099-17110.

Trentmann, J., G. Luderer, T. Winterrath, M. D. Fromm, R. Servranckx, C. Textor, M. Herzog, H.-F. Graf, M. O. Andreae (2006), Modeling of biomass smoke injection into the lower stratosphere by a large forest fire (Part I): reference simulation, *Atmos. Chem. Phys.*, 6, 5247-5260.

Trepte, C. R. and M. H. Hitchman (1992), Tropical stratospheric circulation diagnosed in satellite aerosol data, Nature, **355**, 626-628.

U.S. Forest Service (2004), California Fire Siege 2003: The Story, Government Document A 13.2:C 12/8. U.S. Forest Service, Washington, D.C.

Wang, P. K. (2007),The Thermodynamic Structure atop a Penetrating Convective Thunderstorm. *Atmospheric Research*, *83*, 254-262.

Webb, R., C.J. Davis, and S. Lellyett (2004), Meteorological Aspects of the ACT Bushfires of January 2003, in *2004 Bushfires Conference*, Adelaide, Australia.

Westerling, A. L., Hidalgo, H. G., Cayan, D. R., Swetnam, T. W. (2006), Warming and earlier spring increase western US forest wildfire activity, *Science*, **313**, 940-943.

Yue, G. K., R. E. Veiga, and P. Wang (1994), SAGE II observations of a previously unreported stratospheric volcanic aerosol cloud in the northern polar summer of 1990, *Geophys. Res. Lett.*, **21(6)**, 429–432.

Acknowledgements. We thank Gian Paul Gobbi and the ISAC-CNR Rome group for Frascati lidar data, Peter Englefield for Canada fire-location data, and Chuck McHugh for USFS fire data. The Haute Provence lidar data used in this publication were obtained as part of the Network for the Detection of Atmospheric Composition Change (NDACC) and are publicly available (see http://www.ndacc.org). The early-night measurement at Garmisch-Partenkirchen in Fig. 4 was made by H. Jäger. MDF was supported by NRL internal funding (from the Office of Naval Research). The views, opinions, and findings in this report are those of the authors, and should not be construed as an official NOAA and or U.S. Government position, policy, or decision. Radiosonde-derived data were accessed from http://weather.uwyo.edu/upperair/sounding.html. The authors gratefully acknowledge the NOAA Air Resources Laboratory (ARL) for the provision of the HYSPLIT transport and dispersion model and/or READY website (http://www.arl.noaa.gov/ready.html) used in this publication.

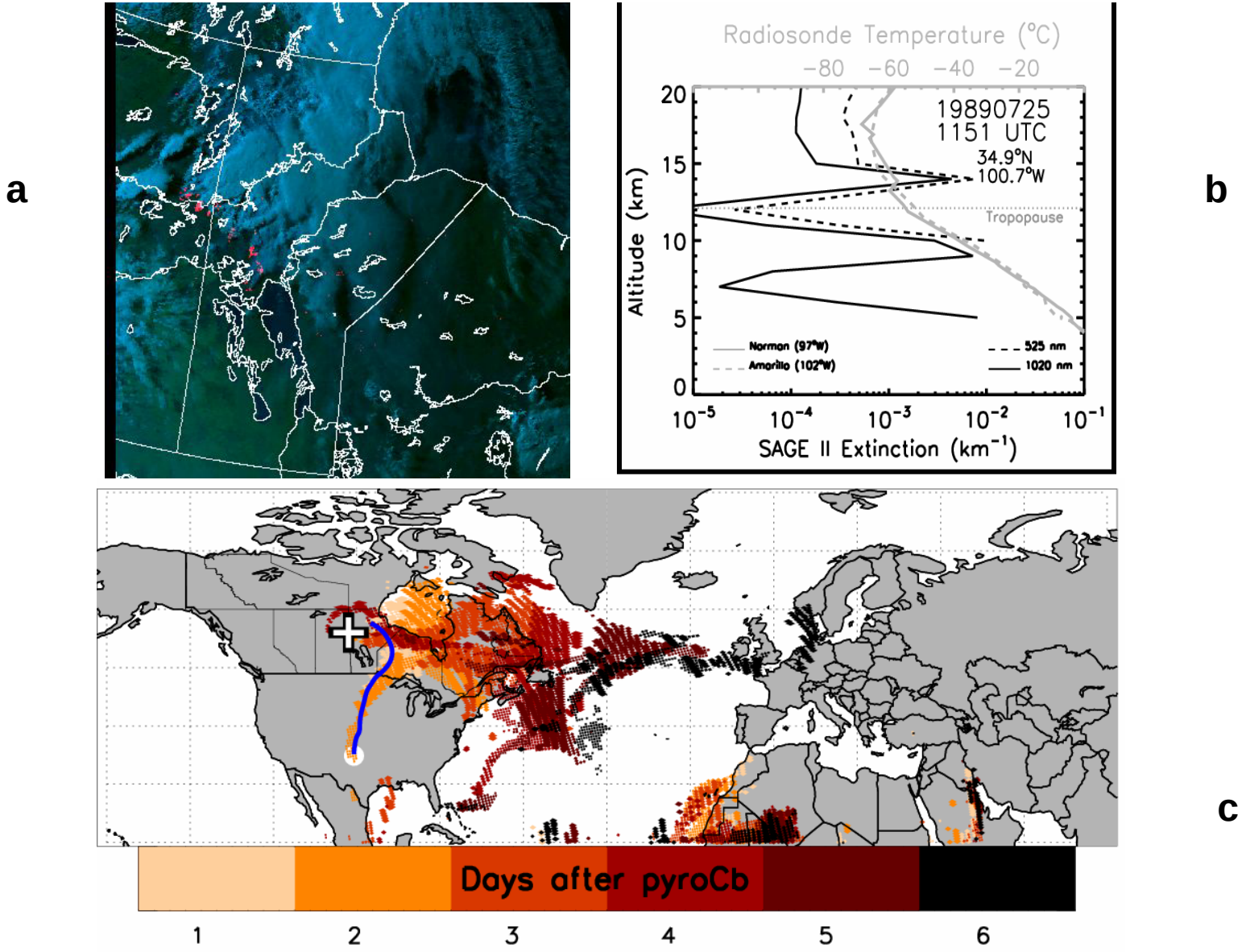

Figure 1. Composite of AVHRR, aerosol index (AI), SAGE layer, and trajectory for 1989 Manitoba and Saskatchewan pyroCbs.
(a)AVHRR false-color rendering of 3.7, 0.86, and 0.63μm radiance for local evening 21 July 1989.
(b) SAGE II aerosol extinction profile.
(c) Map of TOMS AI color coded by date, between 22 and 27 July 1989, location of pyroconvection (+),
the SAGE profile location (white dot), and trajectory (blue line) at SAGE-layer altitude ending 00 UTC 22 July.

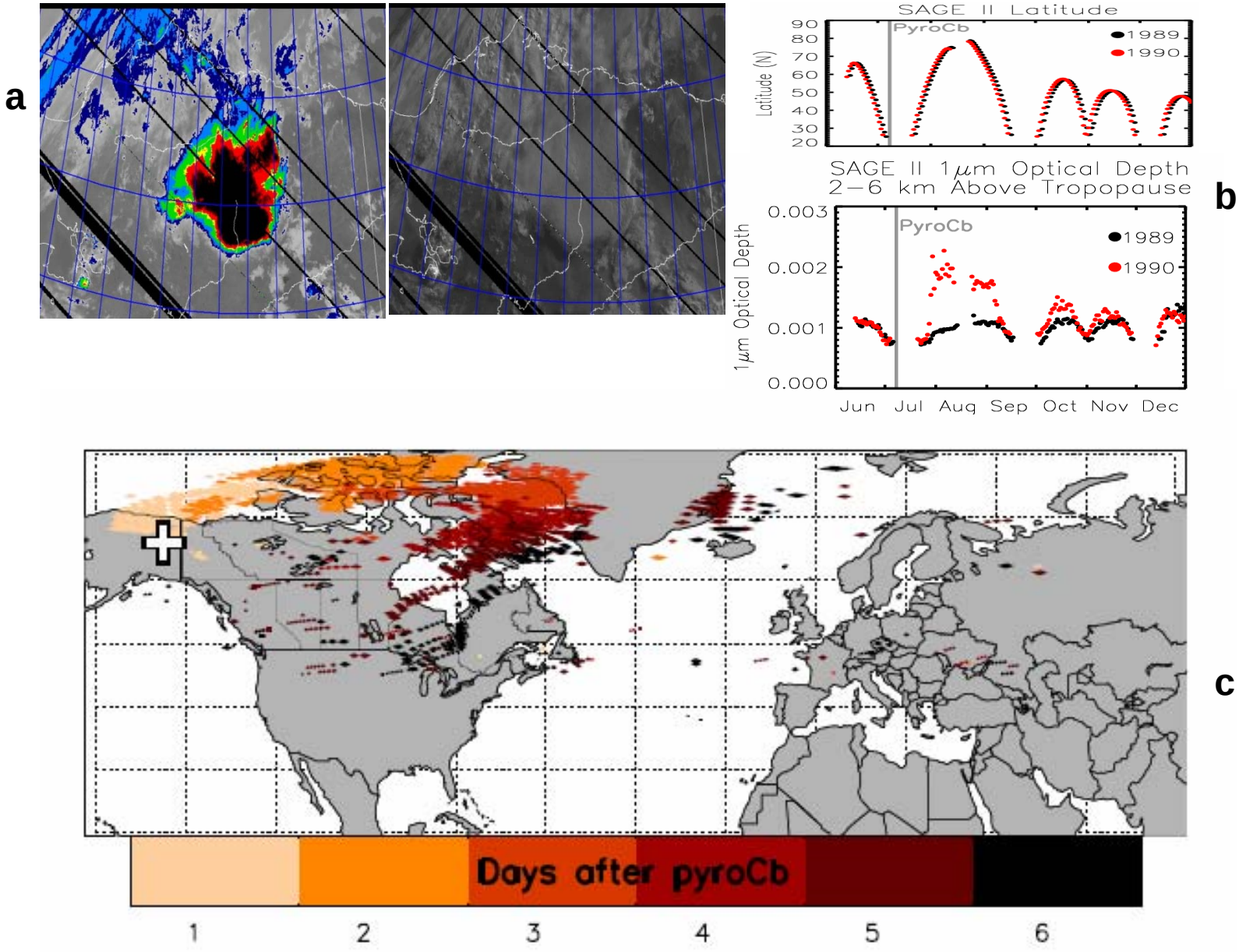

Figure 2. Composite of AVHRR, AI, and SAGE AOD for 1990 Circle pyroCb. (a) AVHRR 11 μm brightness temperature and 0.63μm reflectance image for local evening 6 July 1990 over northern Alaska. IR color enhancement shows BT < -40°C.
(b) SAGE II measurement-latitude pattern for 1989 and 1990 (top) and daily average LS AOD (bottom) for June through December.
(c) Map of TOMS AI color coded by date, between 7 and 12 July 1990 and location of pyroconvection (+).

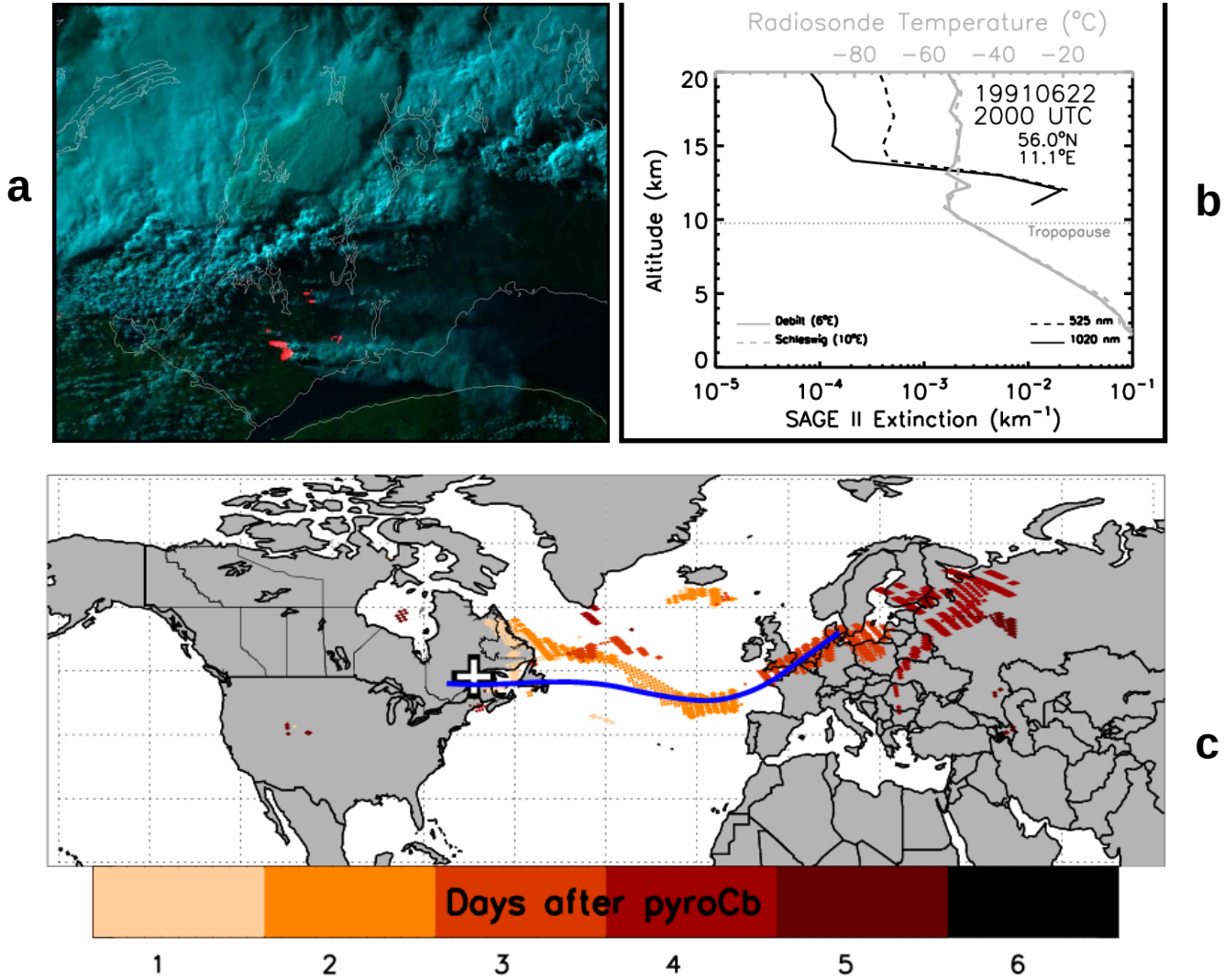

Figure 3. Composite of AVHRR, AI, SAGE layer, and trajectory, for 1991 Quebec pyroCbs.
(a)AVHRR false-color rendering of 3.7, 0.86, and 0.63µm radiance for local evening 19 June 1991.
(b) SAGE II aerosol extinction profile.
(c) Map of TOMS AI color coded by date, between 20 and 25 June 1991,
location of pyroconvection (+), and trajectory (blue line) at SAGE-layer altitude ending 00 UTC 20 June.

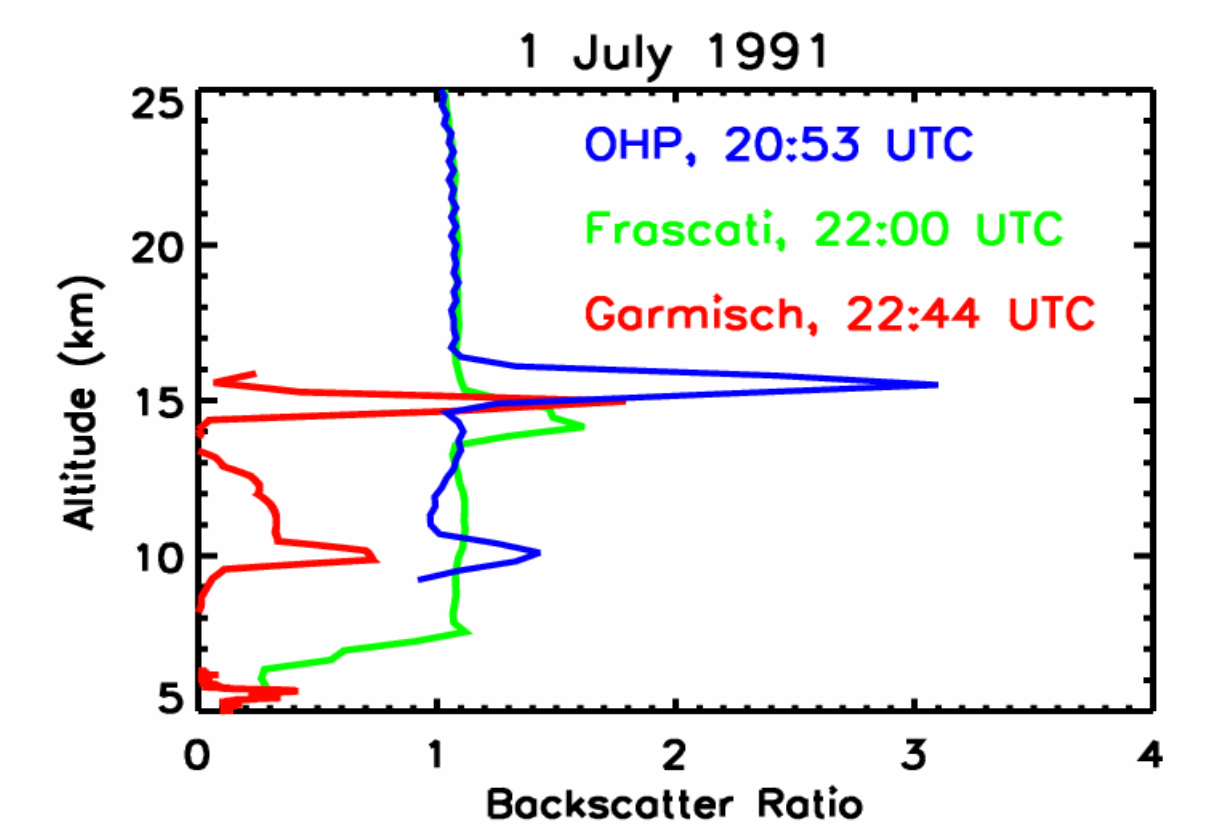

Figure 4. Three European lidar aerosol layers on 1 July 1991, at Haute Provence, France (blue), Frascati, Italy (green), and Garmisch-Partenkirchen, Germany (red).

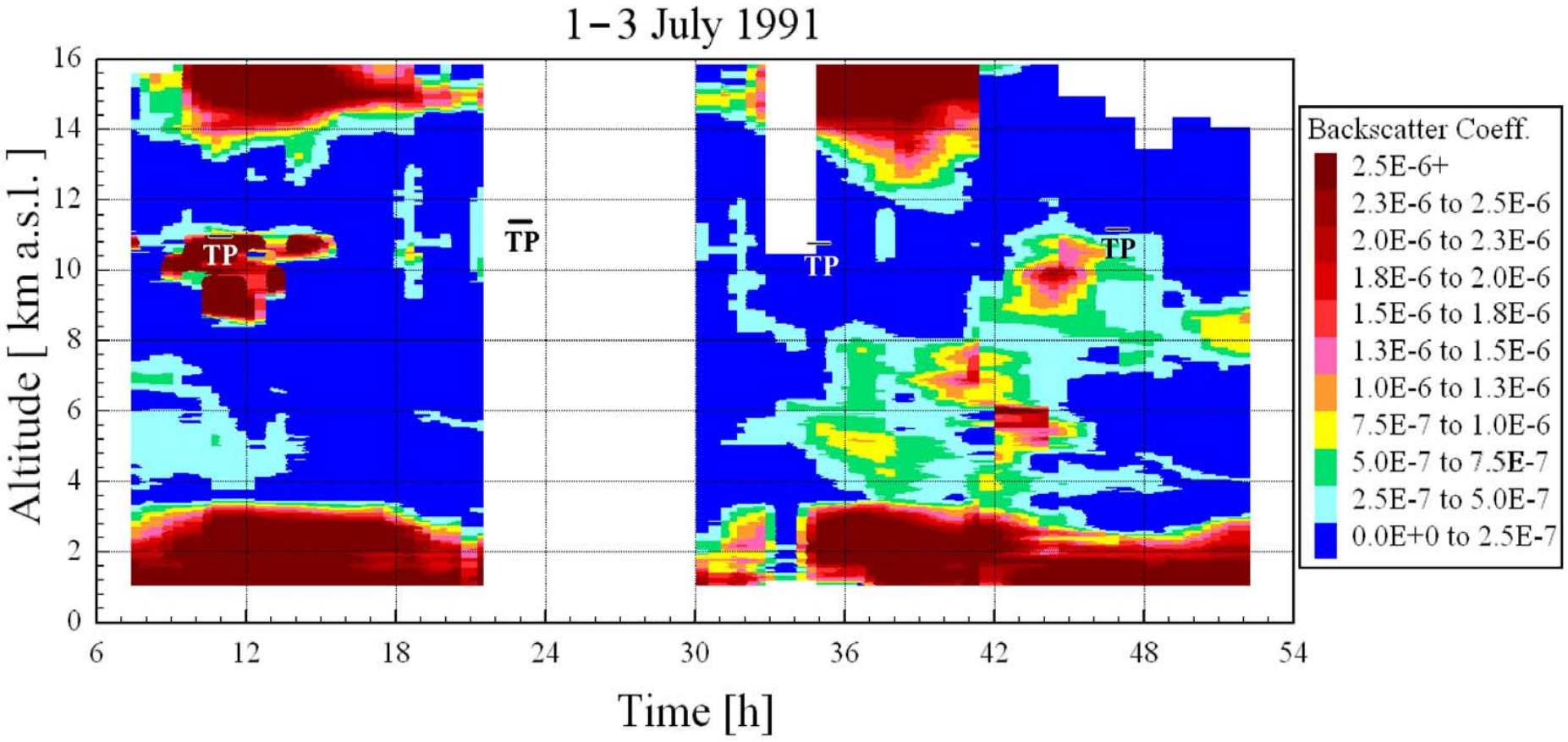

Figure 5. Color-coded time series of the 313-nm backscatter coefficient derived from lidar measurements at Garmisch-Partenkirchen on 1-3 July 1991; the time is given in Central European Time (= UTC + 1 h). Tropopause height from Munich radiosondes annotated as black horizontal line segments over "TP." White-out areas indicate no measurements (22-29 CET) or measurements not possible (e.g. due to clouds).

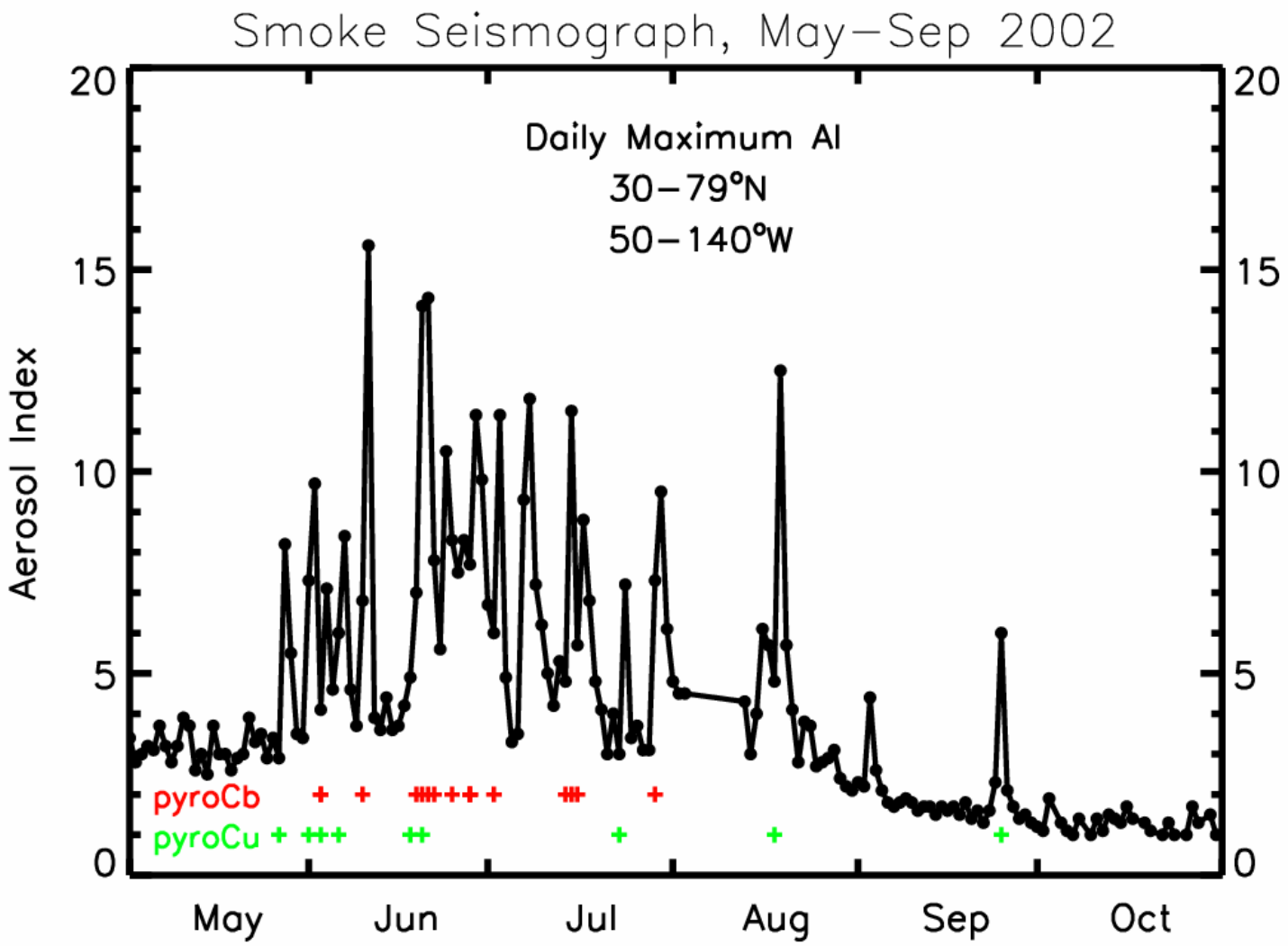

Figure 6. Smoke Seismograph for 2002. Daily maximum NASA TOMS aerosol index over North America, May-October. Annotations for dates of pyroCu (green) and pyroCb (red).

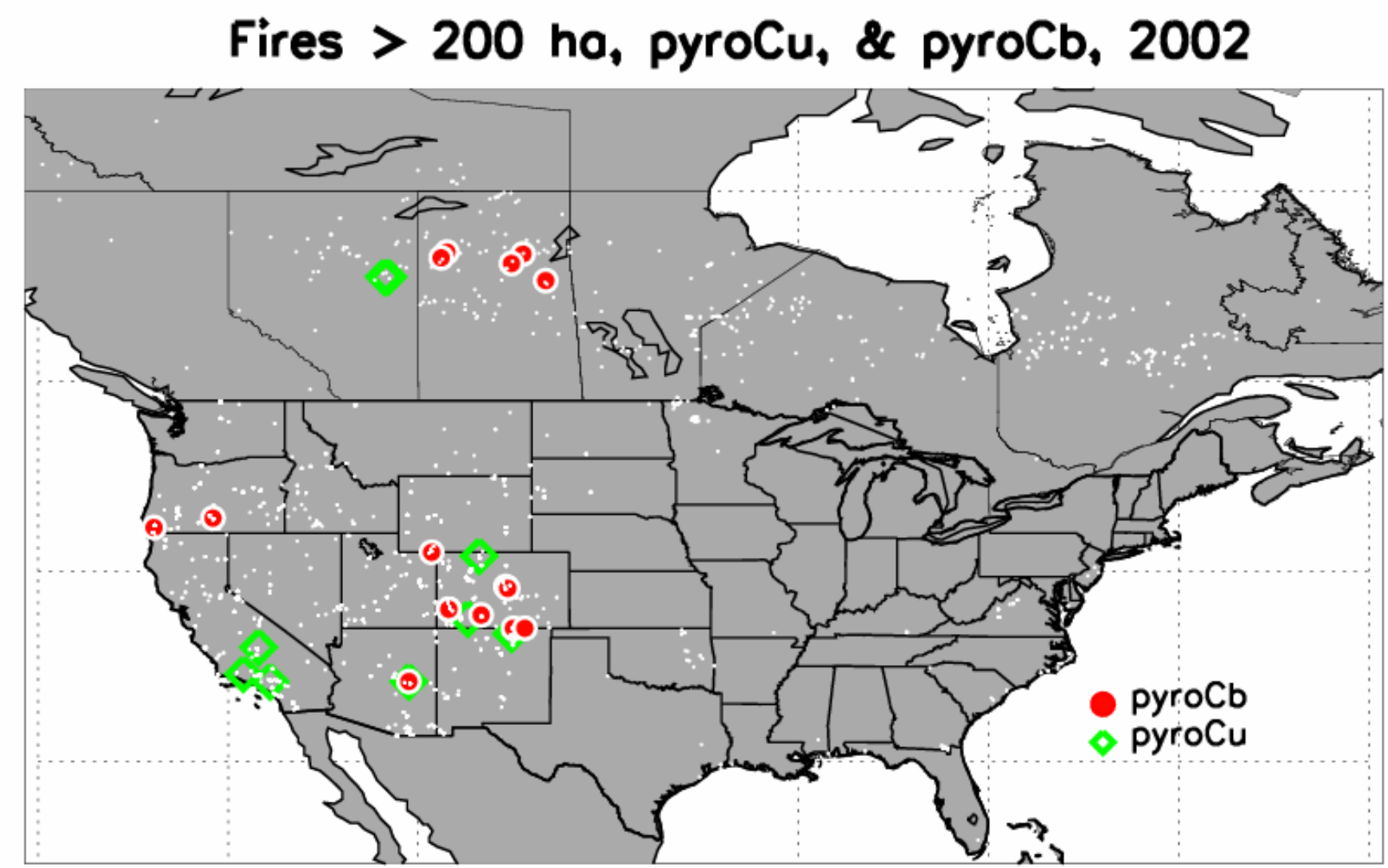

Figure 7. Map of 2002 pyroCu (green diamonds), pyroCb (red filled circles), and Canada/USA fires > 200 ha (white dots).

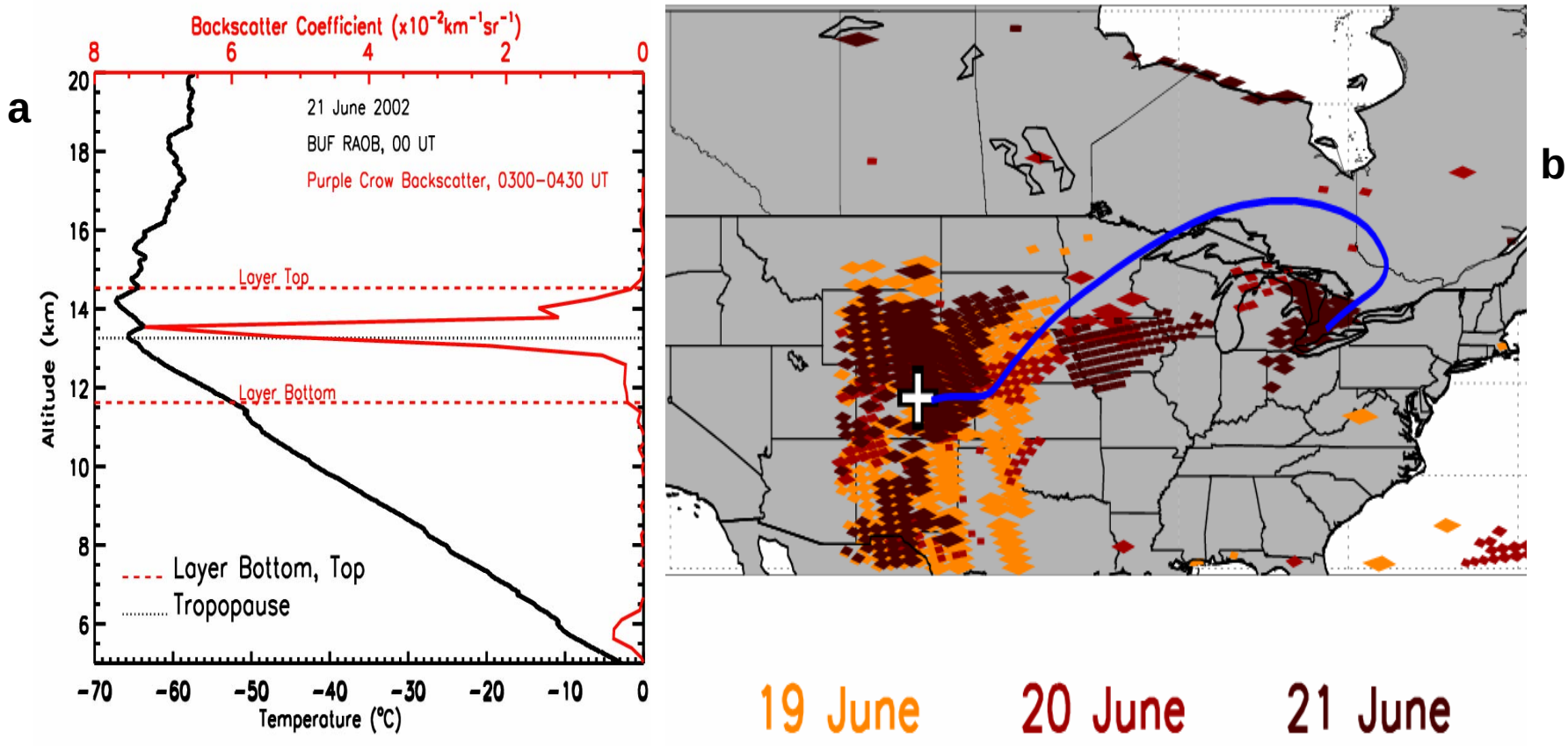

Figure 8. Purple Crow lidar aerosol backscatter, 21 June 2002 and Buffalo radiosonde temperature profile, 21 June 00 UTC. Back trajectory superimposed on AI map like Figures 1-3. Back trajectory altitude is 13 km and endpoint is 19 June, 00 UTC.

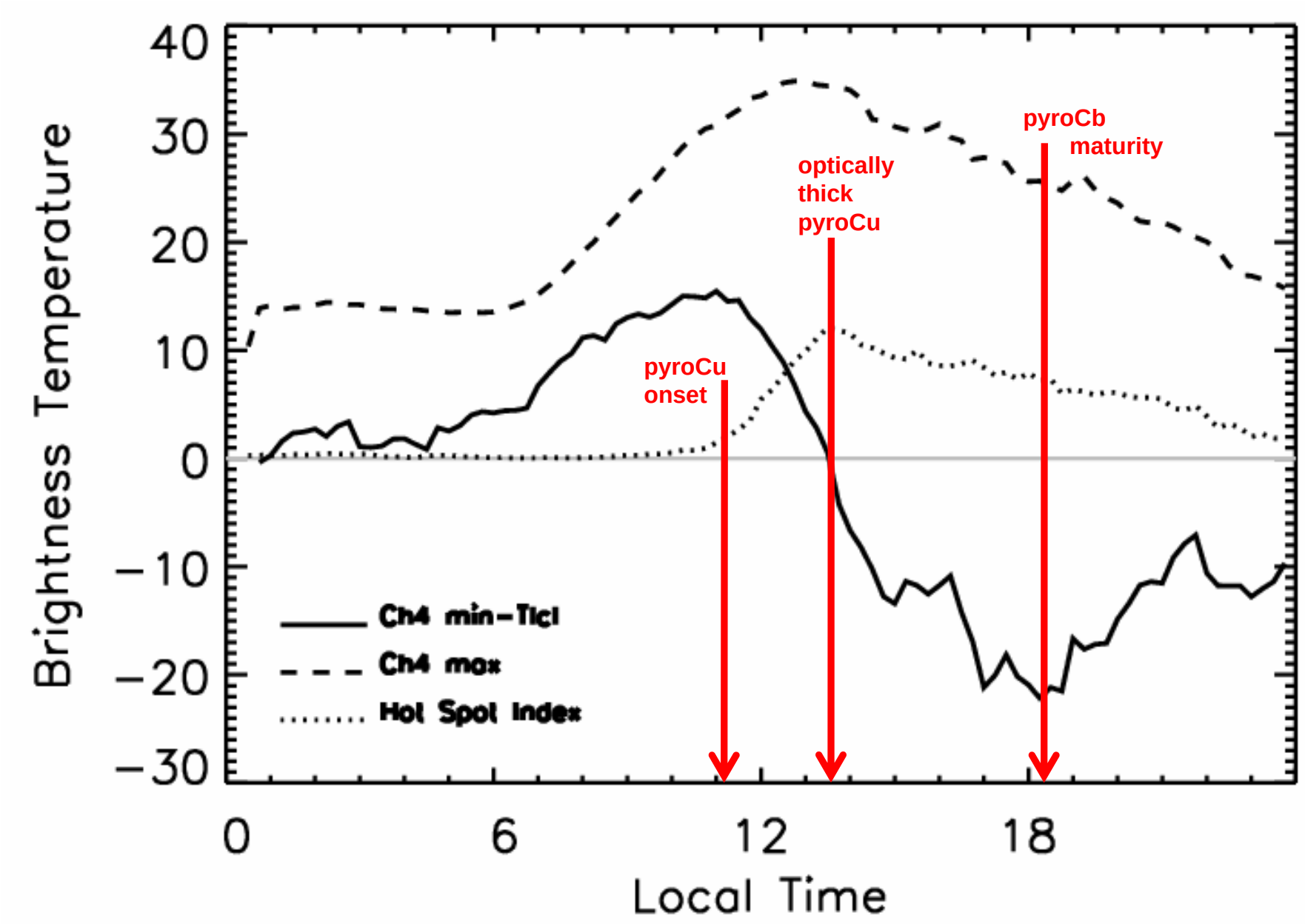

Figure 9. Average diurnal cycle for fire and pyrocloud for 16 pyroCb events in 2002. See text for pixel box used.
Hot spot index is a count of hot spot pixels relative to the maximum observed (dotted line).
11um BT maximum in the box (dashed line); 11um BTmin-LCL temperature (solid black line).